New Journal of Physics
The open-access journal for physics

On mechanisms of interaction in electrosurgery

Daniel Palanker[1,2,4], **Alexander Vankov**[3] **and Pradeep Jayaraman**[1]

[1] Hansen Experimental Physics Laboratory Stanford University, Stanford, CA, USA
[2] Department of Ophthalmology, Stanford University, Stanford, CA, USA
[3] PEAK Surgical Inc., Palo Alto, CA, USA
E-mail: Palanker@stanford.edu

New Journal of Physics **10** (2008) 123022 (15pp)
Received 12 August 2008
Published 16 December 2008
Online at http://www.njp.org/
doi:10.1088/1367-2630/10/12/123022

Abstract. Electrosurgery is broadly used in a wide variety of surgical procedures, yet its underlying mechanisms of interaction are poorly characterized. Fundamentals of electrosurgery have not changed much since the 1930s—cutting is still performed using continuous RF waveforms, leaving a collateral damage zone of hundreds of micrometers in depth. Pulsed waveforms with variable duty cycle are used mostly for tissue coagulation. Recently, we have demonstrated that electrosurgery with microsecond bursts applied via microelectrodes can provide cellular precision in soft tissue dissection. This paper examines dynamics of pulsed electrical discharges in conductive medium, and accompanying phenomena, such as vaporization, cavitation and ionization. It is demonstrated that ionization of the vapor cavity around the electrode is essential for energy delivery beyond the vaporization threshold. It is also shown that the ionization threshold voltage and resistance of the plasma-mediated discharge are much lower in the negative phase of the discharge than in the positive one. Capacitive coupling of the ac waveform to the electrode compensates for this asymmetry by shifting the medium voltage on the electrode, thus increasing the positive and decreasing the negative amplitudes to achieve charge balance in the opposite phases. With planar insulated electrodes having exposed edges of 12.5 μm in width and bursts of 40 μs in duration even tough biological tissues can be dissected with cellular precision. For example, cartilage dissection is achieved with pulse energy of 2.2 mJ per millimeter of length of the blade, and leaves a thermal damage zone of only 5–20 μm in width.

[4] Author to whom any correspondence should be addressed.

Contents

1. Introduction 2
2. Materials and methods 3
3. Results and discussion 3
4. Conclusions 12
Acknowledgments 12
Appendix 13
References 14

1. Introduction

Electrosurgery is one of the most common surgical technologies, and is used in up to 50% of all surgical procedures [1, 2]. Fundamentals of electrosurgery have not changed much since William Bovie's radiofrequency (RF) generator [3]—cutting is still performed using continuous RF waveforms, which thermally ablate soft tissue leaving a collateral damage zone of 100–400 μm [4]. Recent improvements in stabilization of the output power based on monitoring the tissue impedance help to maintain constant cutting and coagulation rates in variable conditions at the electrode–tissue interface, but does not significantly change the extent of associated thermal damage [4, 5]. Pulsed waveforms with variable duty cycle are used only for tissue coagulation [5].

The basic mechanism of tissue ablation and dissection in electrosurgery involves Joule heating of the conductive tissue by electric current, that leads to vaporization and ionization of the water content in the tissue adjacent to the electrode, and ultimately to vapor expansion and tissue fragmentation [4, 5]. Light emission by the plasma is composed primarily of the spectral lines of Na, H, OH and metal ions [6]. Tissue heated below the vaporization threshold remains in place, but can undergo thermal denaturation, with its extent determined by the temperature levels and duration of the hyperthermia. The depth of heat penetration into tissue is determined by the distribution of electric field (source of heating) and by thermal diffusion. Penetration of electric field into the tissue is determined primarily by the size and shape of the electrodes, whereas the extent of thermal diffusion is determined also by the pulse duration. To confine the collateral damage zone in tissue, both these factors should be minimized.

As we described earlier [7], pulses much shorter than the typical lifetime of cavitation bubbles (a few microseconds) induce significant mechanical damage, and thus should be avoided. On the other hand, pulses longer than about 100 μs result in heat diffusion deeper than the cellular size (7 μm). Thus the optimal range of pulse durations for precise electrosurgery is from a few to a few hundred microseconds.

We have recently demonstrated that application of such pulsed waveforms via microelectrodes indeed results in tissue dissection with the damage zone not exceeding a cellular scale [7]–[9]. In this paper, we describe the mechanisms of interaction in pulsed electrosurgery, including dynamics of vaporization, cavitation and ionization, and discuss ways of optimization of the electrical waveforms and electrode geometry for general surgery.

2. Materials and methods

Several pulse generators have been utilized in these studies. Direct current (dc) discharges have been provided by the switching pulse generator (DEI-PVX-4150, Directed Energy Inc, Fort Collins, CO) with the pulse duration controlled by a digital delay/pulse generator DG535 (Stanford Research Systems Inc, Sunnyvale, CA) and high voltage supplied by Xantrex HV bipolar power supply (XHR 600-1.7, Xantrex Technology Inc, Burnaby, BC, Canada). For the alternating current (ac) discharges, we used a home-made pulse generator with a carrier frequency varying from 0.1 to 4 MHz, and burst durations varying from a single cycle to a continuous waveform. All the pulse generators provided square waveforms with rapid (20 ns) switching between the rail voltages varying from ± 100 to ± 700 V. We studied discharges on wire electrodes with diameters from 10 to 100 μm, as well as on home-made blade electrodes with insulated flat sides and exposed edges, made of a tungsten foil of 12.5 μm in thickness, described in detail below. Light emission by the plasma was detected using a photomultiplier (PR-1405RF, Products for Research Inc, Danvers, MA). Voltage and current signals were recorded on a digital oscilloscope (TDS3034 Tektronix, Beaverton, OR).

Discharges were produced in the standard balanced salt solution (BSS PLUS, Alcon Laboratories Inc, Fortworth, TX), with a large (several cm^2) copper foil serving as a return electrode. Fast shadow photography of the cavitation bubbles was performed using an LED flash driven by a home-made current generator, and the images were captured with a liquid nitrogen-cooled CCD camera (LN512, Photometrics, Tucson, AZ).

In experiments with variable temperature of the medium, a glass flask with the electrolyte was placed on a heating stage, and covered to prevent water loss due to evaporation. Temperature was monitored by a thermocouple immersed in the medium. To maintain uniformity of temperature across the flask, an insulated magnet was rotating in the flask at all times. Temperature increased and decreased with a rate of approximately 2 degrees min^{-1}.

3. Results and discussion

Discharge produced on a 50 μm wire electrode of 1 mm in length using direct current in saline exhibited three distinct phases: (i) water heating with nearly constant ionic current through the physiological medium; (ii) vaporization of the medium around the electrode leading to isolation of the metal from the conductive fluid, which manifests itself in impedance increase, and corresponding decrease in current; and (iii) ionization of the vapor around the electrode that allows maintaining the current through the vapor cavity. Two examples of the voltage, current and plasma emission waveforms are shown in figure 1. Dynamics of ionization and plasma-mediated discharge in the positive and negative polarities was found to be very different: in positive discharge, when the metal wire is an anode, the current is stabilized at much lower level than the initial ionic current. In the negative polarity though, the plasma discharge intensifies over time with the current eventually exceeding the initial current through the medium. It should be noted that even though the voltage was set to 430 V on the power supply, the output voltage varied somewhat during the discharge due to inability of the pulse generator to provide sufficient current, as shown in figure 1.

Photographs of the corresponding plasma discharges further exemplify the differences: positive discharge produces a faint cylindrical layer of plasma around the wire electrode, whereas the negative discharge appears as a very bright sphere at the end of the wire.

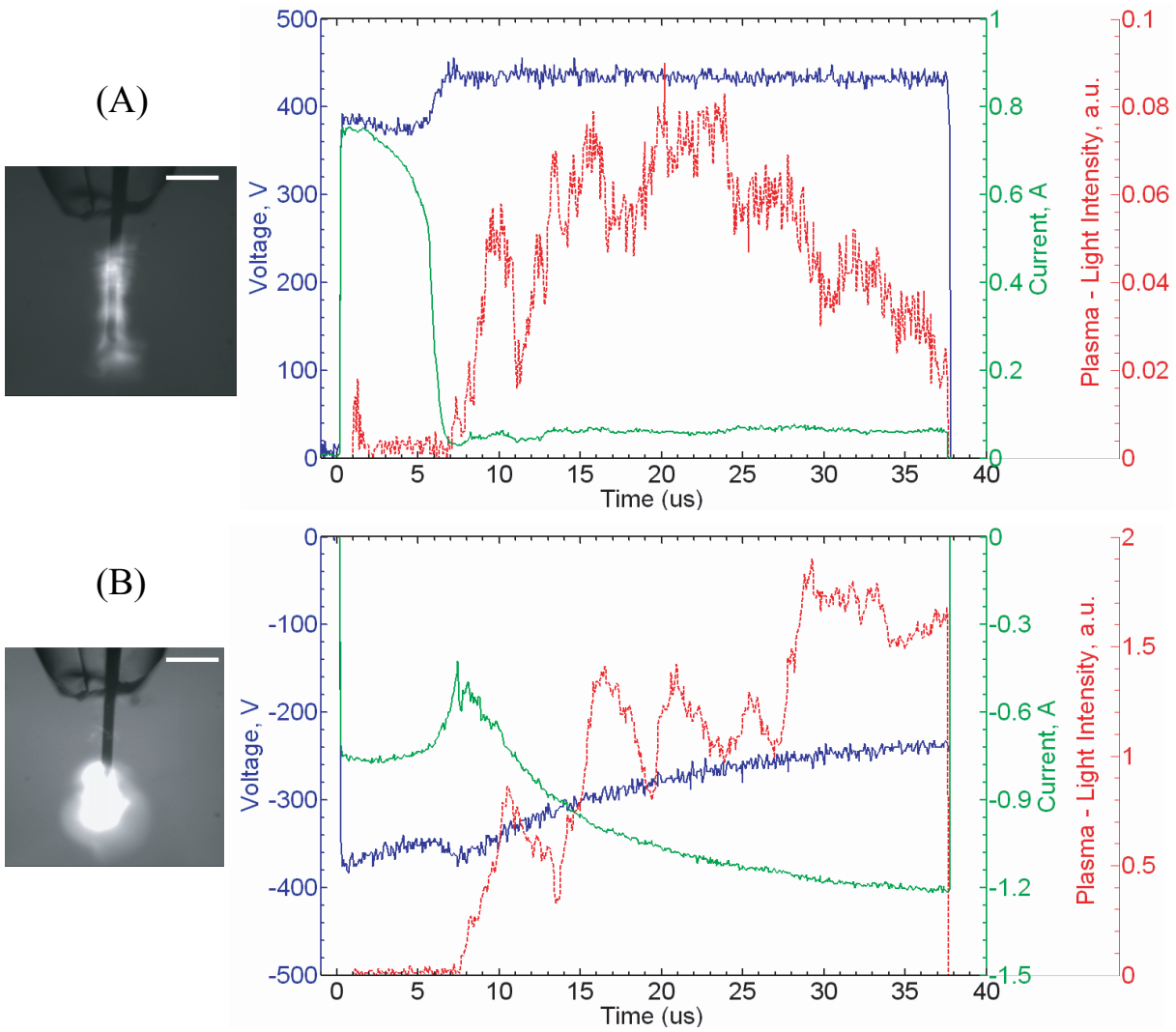

Figure 1. Waveforms of the voltage (blue), current (green) and light emission (red) during the discharge on a wire electrode of 50 μm in diameter in saline. A large return electrode is placed several cm away. Photographs of the discharge integrated over one burst are shown on the left. Scale bars are 250 μm. (A) Anodal discharge (positive voltage on the wire electrode). (B) Cathodal discharge.

We assessed the thresholds of the ionization in positive and negative polarities by measuring the time lag from the beginning of the pulse until the moment of significant vaporization, and then ionization of the vapor around the electrode in both polarities. The results are summarized in figure 2. The moment of significant vaporization was defined as a decrease in electric current by 30%. Ionization threshold was defined as light emission exceeding the PMT noise level by a factor of 5. As one can see in figure 2, at high voltages, ionization in both polarities occurs a few microseconds after the vaporization. However, when voltage decreases toward +300 V, the ionization time in positive polarity rapidly increases, and reaches 100 μs at 280 V. Similarly, delay between vaporization and ionization is rapidly increasing in negative polarity when voltage decreases below −100 V, and exceeds 100 μs at −90 V.

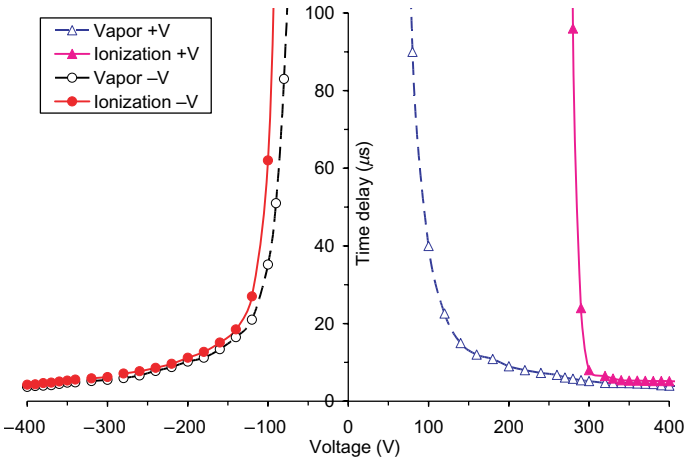

Figure 2. Time lag from the beginning of the pulse until occurrence of vaporization and ionization, as a function of voltage for anodal and cathodal discharges. Vaporization was defined as a moment when electric current is decreased by 30%. Ionization—by light emission exceeding the dark noise by a factor of 5.

Asymmetry in ionization thresholds and dynamics of the plasma-mediated discharges between metal electrode and electrolyte at different polarities has been previously observed [10, 11]. One mechanism that might be responsible for such asymmetry could be the difference in electron ejection from metal versus the liquid [12, 13]. However, the detailed analysis of the mechanisms of ionization is beyond the scope of this study.

The dc discharge is not practical for electrosurgery due to the strong muscle and nerve stimulation, as well as electrolysis of water leading to generation of a large amount of gas. At cycle durations much shorter than the cellular polarization time (of the order of 0.2–5 μs [14]), the direct effects of electric field on cellular membranes are strongly suppressed [7]. So in practice the electrosurgical waveforms are of alternating polarity in the frequency range of 0.2–4 MHz [15]. We studied the effect of the alternating polarity on dynamics of ionization of the water vapor using the waveforms with the carrier frequency of 4 MHz. As shown in figure 3, there can be distinguished the same three phases of the discharge: heating, vaporization and plasma-mediated discharge. Current in the positive and negative polarities remains similar until the beginning of ionization. During the plasma discharge though, similarly to the dc case, the current in the negative phase is much stronger than that in the positive polarity. Light emission by the plasma is also much more intense during the negative phase (figure 3(C)). Thus, even though the alternating polarity voltage waveform is symmetric, the current during the plasma-mediated discharge is largely asymmetric, flowing predominantly during the negative phase. Average current after demodulation of the carrier frequency is shown as a bold red line in figure 3(B). Such rectification of the driving voltage waveform into predominantly direct current can cause significant effects of electric field on the cell membranes, such as stimulation and electroporation.

A common solution for balancing the charge injection into the tissue (as well as a safety precaution) is a separating capacitor. Coupling the ac waveform to the electrode via a 1.4 nF capacitor results in the initial charging of the capacitor with the unbalanced current at the

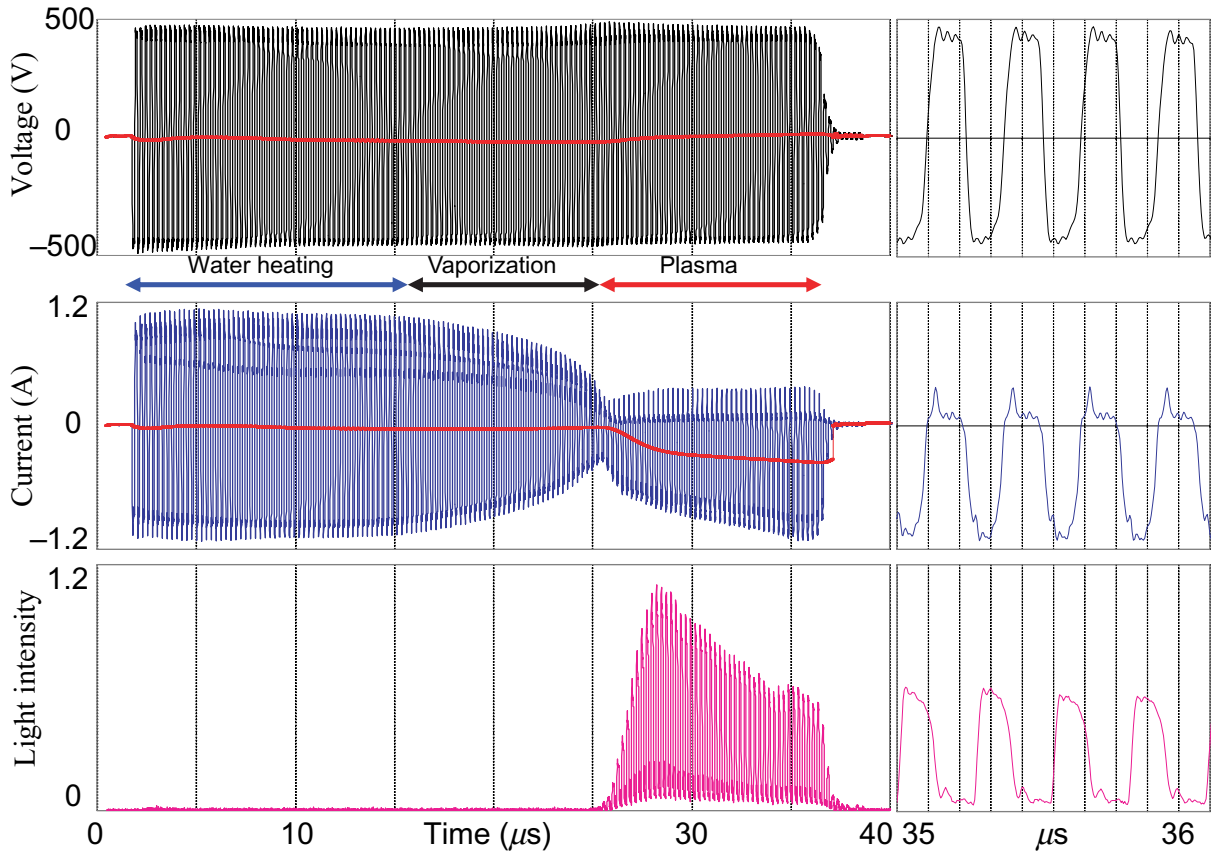

Figure 3. Waveforms of voltage (top), current (middle) and light emission (bottom) of a 4 MHz ac discharge on a 50 μm wire electrode in saline. 1 μs long fragments of the waveforms are shown on the right. Demodulated medium voltage and current are shown as a red line in the upper two graphs. The vaporization phase begins when the current starts decreasing, indicating decrease in the metal–liquid interface area. The ionization phase is marked by emission of light.

beginning of the plasma-mediated discharge (30–33 μs on figure 4). This charging leads to increase of the voltage amplitude during the positive phase and corresponding decrease during the negative phase (figure 4(A)), which results in more balanced currents during the opposite phases of the cycle. Within a few microseconds, balance is achieved, and the waveforms stabilize until the end of the burst. Interestingly, even though the charge balance is now maintained, the plasma remains brighter during the negative phase, as can be seen in the figure 4(C). The separating capacitor discharges its excess net charge after termination of the burst. However, since the vapor still isolates the electrode at the end of the pulse, and there is no plasma in the absence of high voltage, the discharge of the residual voltage is quite slow—several microseconds.

The positive and negative polarity thresholds are shown in figure 4 as dashed green horizontal lines. Initial asymmetry of the conductivity in the positive and negative phases of the plasma-mediated discharge will shift the medium voltage into the balanced state, i.e. when charge injection in each phase is equal. To sustain a stable plasma-mediated discharge, the

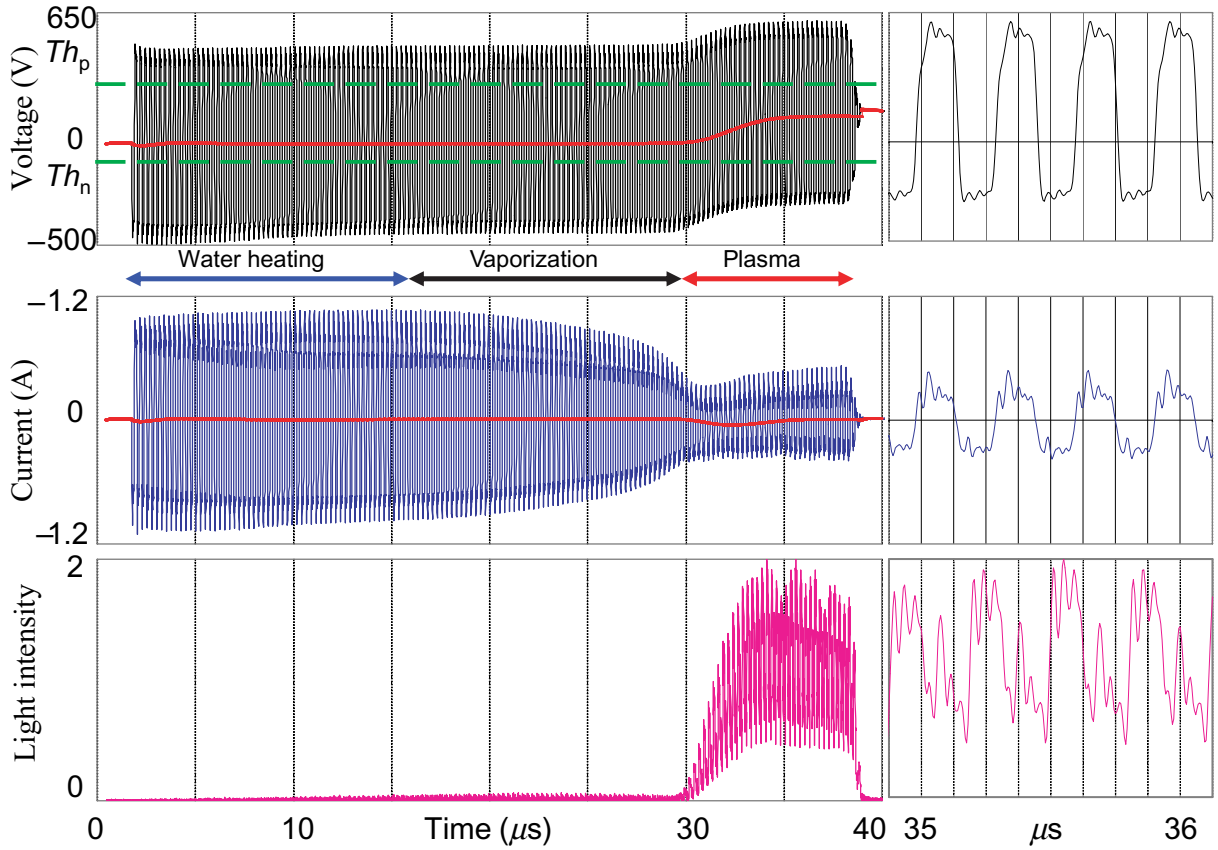

Figure 4. Waveforms of voltage (top), current (middle) and light emission (bottom) of a 4 MHz ac discharge with a 50 μm wire electrode coupled via a 1.4 nF capacitor. One microsecond long fragments of the waveforms are shown on the right. Demodulated medium voltage and current are shown as red lines in the upper two graphs. Ionization threshold voltages for anodal and cathodal phases are shown as green dashed lines in the upper plot.

voltage in such steady state should exceed the positive and negative thresholds. This means that the amplitude A of the ac voltage waveform should exceed the average of the two thresholds: $A > (Th_p - Th_n)/2$. For example, for $Th_p = 280$ V and $Th_n = -100$ V, the amplitude of the waveform should exceed 190 V. This estimate matches the previously published ionization threshold voltage measured with a continuous RF signal ($175 < A < 200$ V) [6].

To check whether formation of the gas around the electrode is due to vaporization or electrolysis of water, we measured dependence of the vaporization time on starting temperature of the electrolyte. If gas formation were due to electrolysis, it would not strongly depend on the starting temperature. If it were due to vaporization, the threshold energy would linearly decrease with the starting temperature. Since the power during the heating phase in water is constant, we measured delay time until the current decreased by 30%, as a measure of the deposited energy. To further verify reliability of these measurements we repeated them for 3 levels of voltage: 300, 350 and 400 V. The results are shown in figure 5. Extrapolating the linear fit of the plots to the point of zero delay time (intersection with abscissa) provides an estimate of the vaporization temperature. As one can see in this figure, for all 3 voltages, the threshold

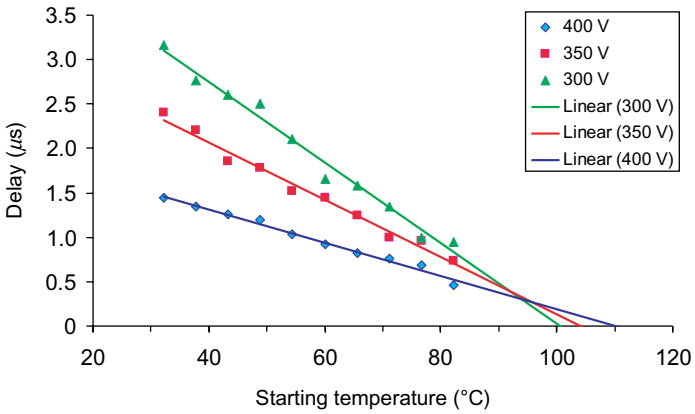

Figure 5. Time lag from the beginning of the pulse until occurrence of gas formation, defined as a moment when electric current is decreased by 30%. This time delay is plotted as a function of the starting temperature of the electrolyte (BSS) for 3 voltage levels: 300, 350 and 400 V. Linear fits are extrapolated to the point of intersection with the abscissa.

temperature is within a range of 100–110 °C. The linear dependence of the threshold energy on starting temperature proves that the gas formation is due to vaporization. However, the threshold temperature is surprisingly low for microsecond heating. In experiments with microsecond laser heating, the vaporization threshold was found to exceed 150 °C. [16]. Lower threshold temperature in our case could be due to abundance of the hydrogen and oxygen microbubbles produced by electrolysis at the electrode–electrolyte interface, which might ease formation of the vapor bubbles by serving as nucleation centers.

To better understand the dynamics of vaporization on a wire electrode, and assess the size and shape of the vapor cavity, we imaged the shadow of the vapor bubble using fast flash photography. LED flash duration was 200 ns. To further help identify the steps of the bubble formation we used a sequence of monopolar pulses applied at 200 kHz. We applied positive voltage just under the ionization threshold, which allowed the dynamics of vaporization to be studied while avoiding more complex interactions involving plasma. As can be seen in figure 6, each pulse in the burst produces a distinct step in the bubble. Due to enhancement of electric field (i.e. current density) at the ends of the cylindrical probe, the bubble starts at the apex (figure 6(A)). When this area becomes isolated by the non-conductive vapor, the adjacent part of the wire becomes an apex with the highest current density. The next pulse vaporizes water around that area, and so on. In addition to propagation of the vapor cavity from the singular end points of the wire, heating of its central part eventually leads to vaporization along the whole wire: as shown in the zoom insert in figure 6(D), by 27 μs, the middle part of the wire becomes covered with a thin layer of vapor. By the end of 30 μs, the first bubble at the apex of the wire is almost collapsed. Since the heating was produced by short (2.5 μs) pulses of positive polarity at voltage close to ionization threshold (310 V), the plasma did not develop during the burst.

Even at voltages significantly exceeding the ionization threshold, plasma does not occur immediately at the beginning of vaporization, but rather only after a significant decrease in the current, i.e. when a significant fraction of the electrode becomes covered by the vapor. The reason for this is the fact that the voltage step across the vapor cavity depends on impedance

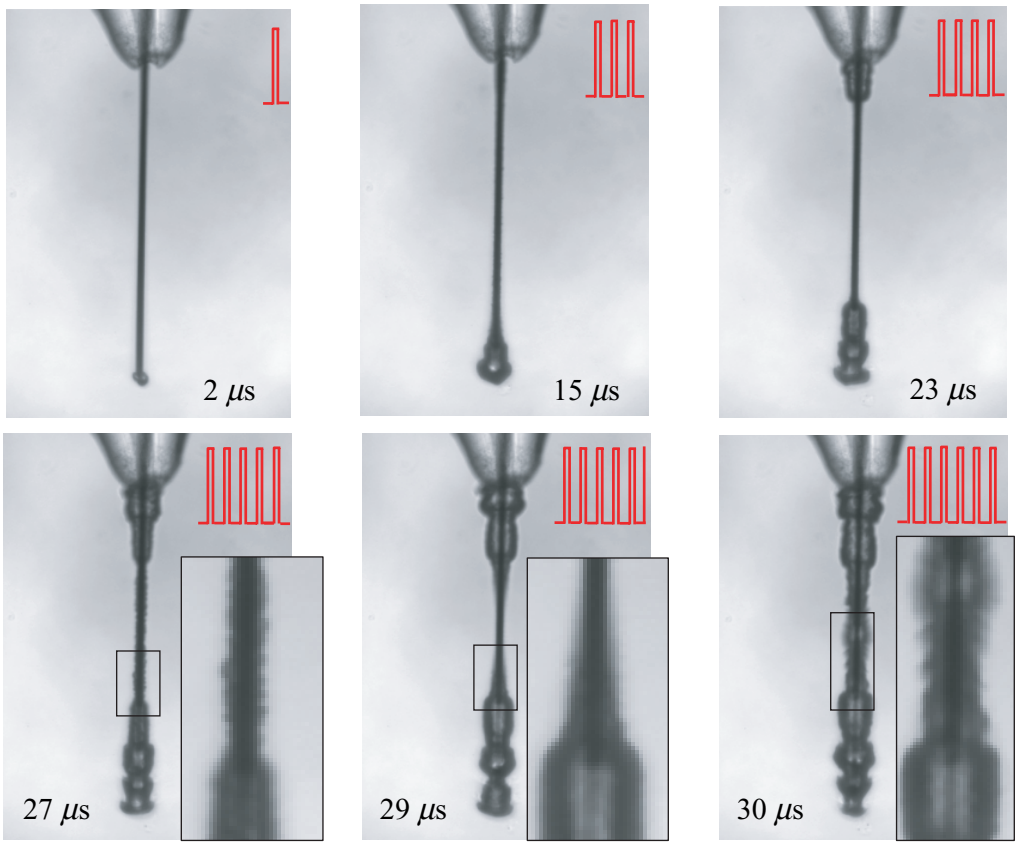

Figure 6. Dynamics of vaporization of saline on a 25 μm wire electrode of 1 mm in length, driven by a 6 pulse dc burst at a carrier frequency of 200 kHz. Voltage amplitude was +310 V, timing of the fast flash (200 ns in duration) and the number of pulses applied are shown in each frame.

of the discharge at the electrode–liquid interface. When a large portion of the electrode is still connected to the liquid, the voltage in the proximity of the electrode in the liquid will not differ very much from the electrode potential. Thus the voltage step across the vapor cavity will be relatively small. As soon as the impedance of the interface with liquid becomes sufficiently high (i.e. exposed area of the electrode becomes sufficiently small), so that the voltage step across the vapor cavity exceeds the ionization threshold, the plasma will start developing. A delay between the occurrence of ionization and vaporization at various voltages can be seen in figure 2.

The penetration depth of the electric field into the tissue and the amount of energy required for vaporization of the surface water layer increase with the electrode radius. Threshold energy of vaporization on a cylindrical electrode with radius r_o and length L can be estimated as: $H = 2 f c \rho \cdot \Delta T \cdot V \cdot \ln \frac{L}{r_o}$ (appendix, equation (A.11)), where $V = \pi r_o^2 L$ is the electrode volume, ΔT is the threshold temperature rise in water, c and ρ are the specific heat capacity and density of water. Form factor f describes deviation of the current waveform from rectangular due to vaporization starting from the end points rather than taking place simultaneously along the whole electrode. Since the threshold energy rapidly (almost quadratically) increases with electrode radius, thinner electrodes should allow for lower energy deposition, and consequently, for reduced collateral damage.

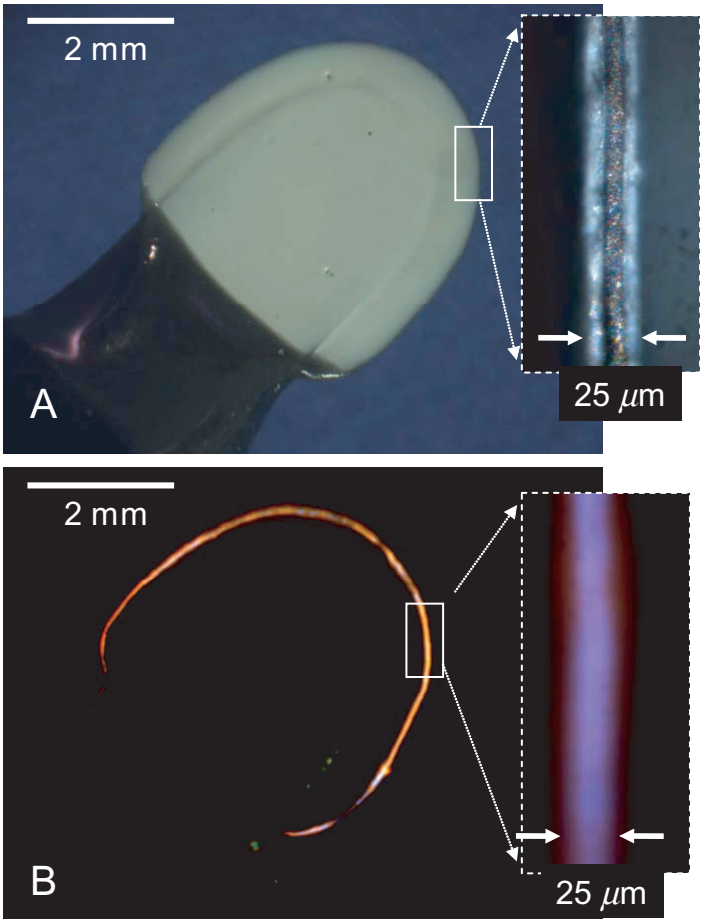

Figure 7. (A) Glass insulated planar electrode for general surgery. Insert shows an exposed edge of 12.5 μm in width. (B) Plasma emission from the exposed edge of the electrode during the discharge.

However, wires thinner than 50 μm are practically invisible to a surgeon, even under a surgical microscope. In addition, thin wire electrodes are just too soft for practical surgical application. To address these difficulties we developed a blade electrode with insulated sides and exposed thin edge, as shown in figure 7. The thickness of the foil electrode was 12.5 μm, and the insulating layer of glass on each surface was about 6 μm in thickness. The central part of the electrode had increased thickness for enhanced mechanical robustness of the blade.

The 4 MHz driving voltage of $\pm$480 V in amplitude, and the corresponding electric current and plasma emission are shown in figure 8. Due to the decreased radius of the electrode, vaporization is complete and ionization started by 3 μs. Two microseconds later the current balance of the plasma-mediated phase is achieved due to the charging of the 1.4 nF separating capacitor, which shifts the medium voltage by approximately 100 V. The rest of the discharge is practically stable until the end of the burst.

As shown in the upper plot in figure 8, partial rectification of the ac waveform during the plasma discharge results in a net positive step of voltage, which is converted by the separating capacitor into two pulses of current: a few microseconds long negative pulse at the beginning of the plasma discharge, and somewhat longer and weaker positive pulse at the end.

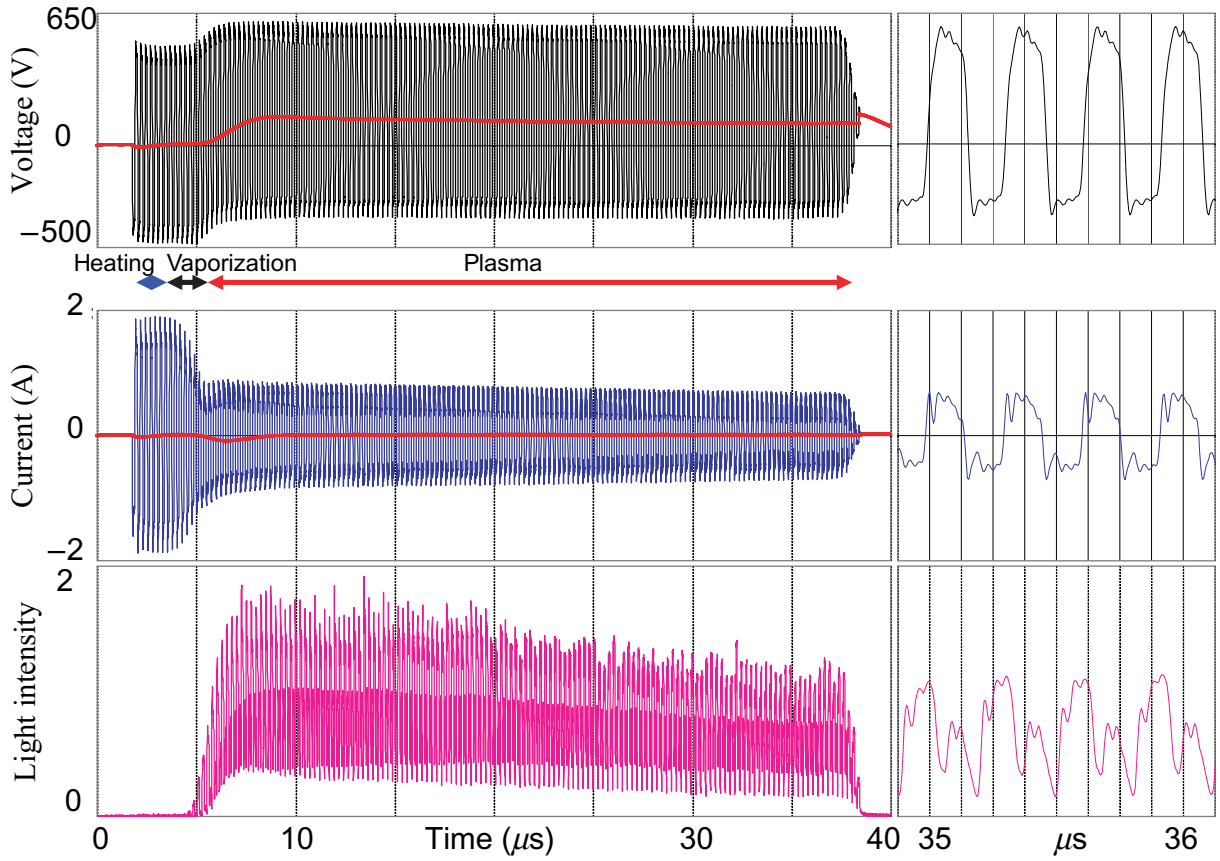

Figure 8. Waveforms of voltage (top), current (middle) and light emission (bottom) of a 4 MHz ac discharge with a blade electrode coupled via a 1.4 nF capacitor. One microsecond long fragments of the waveforms are shown on the right. Demodulated medium voltage and current are shown as red lines in the upper two graphs.

Since these pulses are much longer than the carrier frequency cycle, they may contribute to cellular stimulation much more than the rapidly oscillating electric field at the carrier frequency. Since the thresholds of electroporation and neural stimulation increase with decreasing pulse duration [17, 18], it makes sense to decrease duration of these rectified pulses by applying a smaller separating capacitor. However, the time constant of this filter cannot be decreased below the duration of the carrier cycle, since it would significantly diminish the output power.

To assess the cutting rate and the width of the collateral damage zone in tissue, we applied this blade to several types of biological tissues *in vitro*, including cartilage, skin, muscle and fascia. No cutting was observed below the ionization threshold. Typical waveform used for cutting the cartilage is similar to the one shown in figure 8. Voltage amplitude was ±430 V, burst duration 37.5 μs at 4 MHz. Repetition rate was maintained below 1 kHz to provide sufficient cooling time between the bursts. With a 3.7 mm long blade fully immersed into physiological medium at these settings, the peak power at the beginning of the burst was 522 W, and during the plasma-mediated discharge was 215 W. Total energy deposited during one burst was 8.14 mJ, or 2.2 mJ per millimeter of length of the blade. A typical histological appearance of a cut in

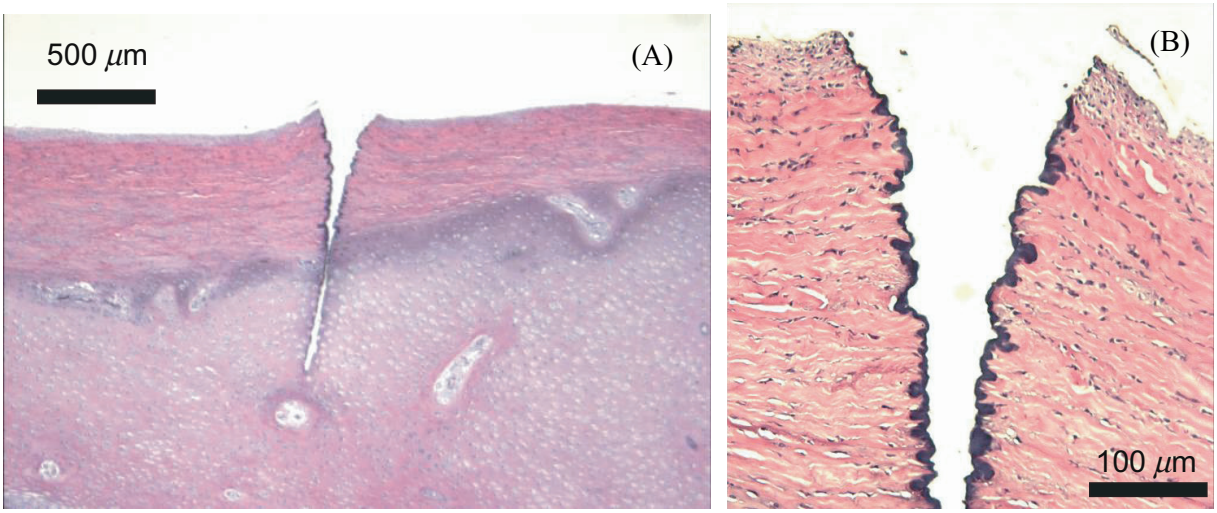

Figure 9. (A) Cut in the perichondrium layer and the hyaline cartilage of porcine knee produced by a blade electrode at voltage amplitude of +/ − 430 V and burst duration of 37.5 μs. (B) Higher magnification view of the fibrous perichondrium layer demonstrating the thermal damage zone (dark staining) of 5–20 μm in width.

porcine knee cartilage produced at the pulse repetition rate of 200 Hz is shown in figure 9. Both the fibrous perichondrium layer and the hyaline cartilage layer are dissected. A higher magnification photograph shown in figure 9(B) demonstrates the width of the thermal damage zone (darker area at the edges of the cut) varying from 5 to 20 μm.

4. Conclusions

We have demonstrated the dynamics of vaporization and ionization during pulsed electrosurgical dissection of biological tissue. Ionization of the water vapor cavity around the electrode is essential for delivery of energy beyond the water vaporization threshold. Resistance of the plasma-mediated discharge and the threshold voltage are much lower in the negative phase of the discharge than in the positive one. Capacitive coupling of the ac waveform to the electrode compensates for this asymmetry by increasing the medium voltage on the electrode, thus increasing the positive and decreasing the negative amplitudes to achieve charge balance in the opposite phases.

With an electrode of 12.5 μm in width and bursts of several tens of microseconds in duration applied at repetition rate of hundreds of Hz, biological tissues can be dissected with cellular precision. For example, cartilage dissection is achieved with pulse energy of 2.2 mJ per millimeter of length of the blade, and leaves a thermal damage zone at the edges of 5–20 μm in width.

Acknowledgments

We thank Roopa Dalal for the histological preparations and photography. This work was supported in part by the NIH grant 2R01 EY012888-04 and by the Air Force Office of Scientific Research (MFEL grant).

Appendix

The energy required for vaporization of water around the electrode prior to plasma formation can be calculated as follows:

$$H = \int_0^{\tau} \frac{U^2}{R} \mathrm{d}t, \tag{A.1}$$

where τ is the time lag of vaporization, U is the voltage and R is the resistance of the discharge. For most of the experiments, we used a constant dc voltage waveform, or ac waveform with a constant amplitude, therefore in order to calculate E_{thresh} one needs to know only the resistance R(t) and time τ.

A.1. Resistance between a cylinder and a large return electrode at infinity

To obtain analytical solution of this problem we will approximate a cylindrical rod of radius r_0 and length $L = 2a$ by an ellipsoid with half-axes a and r_0. An ellipsoid with total charge q induces a potential U in vacuum [19] described as following:

$$U = \frac{q}{2f} \ln \frac{A+f}{A-f}, \tag{A.2}$$

where $f = \sqrt{a^2 - r_0^2}$—is a focal length of the ellipsoid, $A = \sqrt{a^2+\lambda}$, and λ is the parameter of the equipotential surfaces, determined by ellipsoid equation:

$$\frac{x^2}{a^2+\lambda} + \frac{y^2}{r_0^2+\lambda} = 1. \tag{A.3}$$

At the surface of the charged ellipsoid $\lambda = 0$, so equation (A.2) can be simplified:

$$U_0 = \frac{q}{2f} \ln \frac{a+f}{a-f} = \frac{q}{L\sqrt{1-\alpha^2}} \ln \frac{1+\sqrt{1-\alpha^2}}{1-\sqrt{1-\alpha^2}}, \tag{A.4}$$

where α is the inverse aspect ratio of the rod: $\alpha = 2\mathrm{r}_0/L$. Taking into account Gauss theorem $4\pi q = \oint_{\mathrm{S}} \vec{E}\mathrm{d}S$, and the relation between electric field E and current density J in a uniform medium with resistivity γ, $\vec{J} = \vec{E}/\gamma$, one can obtain

$$4\pi q = \gamma \oint_S \vec{J}\mathrm{d}S = \gamma I = \gamma U_0/R, \tag{A.5}$$

where $I = U_0/R$ is the total current from the ellipsoid. Comparing equations (A.4) and (A.5), one can obtain the formula for the resistance of the ellipsoid electrode in conductive medium:

$$R = \frac{\gamma}{4\pi L\sqrt{1-\alpha^2}} \ln \frac{1+\sqrt{1-\alpha^2}}{1-\sqrt{1-\alpha^2}}. \tag{A.6}$$

For a spherical case, when $\alpha = 1$, the formula can be appropriately reduced to $R = \frac{\gamma}{4\pi r_0}$. At very small aspect ratios $\alpha \ll 1$, the formula reduces to

$$R = \frac{\gamma}{2\pi L} \ln \frac{2}{\alpha} = \frac{\gamma}{2\pi L} \ln \frac{L}{r}. \tag{A.7}$$

Electric field at central portion of the probe can be found from equation (A.2) by taking derivative of U with respect to the radius. Since in the center of the ellipsoid $y = 0$, then

$r = x$. From equation (A.3) then follows: $x = \sqrt{a^2 + \lambda} = A$. Taking into account equations (A.5) and (A.7) we obtain:

$$E_{\mathrm{cyl}} = -\left.\frac{\mathrm{d}U}{\mathrm{d}r}\right|_{r=r_0} = -\left.\frac{\mathrm{d}U}{\mathrm{d}A}\right|_{\lambda=0} = \frac{2q}{Lr_0} = \frac{U_0}{r_0 \ln(L/r_0)}. \tag{A.8}$$

A.2. Vaporization time and energy

Conductive medium (saline) is heated by $\Delta T = T_{\mathrm{b}} - T_0$ from the starting temperature T_0 to a vaporization temperature T_{b} during the time t_0 given by

$$t_0 = \frac{c\gamma\rho \cdot \Delta T}{E^2}, \tag{A.9}$$

where c is the specific heat capacity, ρ is the water density. Substituting E from equation (A.8) one can obtain the time required to reach vaporization temperature at the center of the rode:

$$t_{\mathrm{center}} = \frac{c\gamma\rho \cdot \Delta T \cdot r_0^2}{U_0^2} \ln^2 \frac{L}{r_0}. \tag{A.10}$$

For an electrode of 12.5 μm in width and 3.7 mm in length at voltage $U_0 = 430$ V, this formula yields $t = 2.2\,\mu$s. Experimental delay time for these parameters was 2.7 μs.

The energy deposited during that time can be calculated from equation (A.1), using equations (A.7) and (A.10):

$$H = f\frac{U_0^2}{R} t_{\mathrm{center}} = 2 f c\rho \cdot \Delta T \cdot V \cdot \ln \frac{L}{r_0}, \tag{A.11}$$

where f is a form factor, which describes increase of the impedance R over time during vaporization phase, $V = \pi r_0^2 L$—is the volume of the cylindrical electrode.

For the same electrode size at the same voltage, and $f = 0.8$, the formula (A.11) yields $H = 1.6$ mJ. The experimental threshold value for these parameters was 1.8 mJ.

References

[1] Medtech Insight 2007 *US Surgical Procedure Volumes* Report No A606, Medtech Insight LLC, a division of Windhover, Information, Inc. pp 1–2

[2] Medtech Insight 2006 *US Markets for Electrosurgical and Thermal Ablation Products* Medtech Insight LLC, a division of Windhover Information, Inc. p ES-2

[3] Bovie W T 1928 New electro-surgical unit with preliminary note on new surgical-current generator *Surg. Gynecol. Obstet.* **47** 751–2

[4] Brown D B 2005 Concepts, considerations, and concerns on the cutting edge of radiofrequency ablation *J. Vasc. Intervent. Radiol.* **16** 597–613

[5] Massarweh N N, Cosgriff N and Slakey D P 2006 Electrosurgery: history, principles, and current and future uses *J. Am. Coll. Surg.* **202** 520–30

[6] Woloszko J, Stalder K R and Brown I G 2002 Plasma characteristics of repetitively-pulsed electrical discharges in saline solutions used for surgical procedures *IEEE Trans. Plasma Sci.* **30** 1376–83

[7] Palanker D V, Vankov A and Huie P 2008 Electrosurgery with cellular precision *IEEE Trans. Biomed. Eng.* **55** 838–41

[8] Priglinger S G *et al* 2007 Pulsed electron avalanche knife: new technology for cataract surgery *Br. J. Ophthalmol.* **91** 949–54

[9] Priglinger S G *et al* 2005 Pulsed electron avalanche knife (PEAK-fc) for dissection of retinal tissue *Arch. Ophthalmol.* **123** 1412–8
[10] Stalder K R *et al* 2001 Repetitive plasma discharges in saline solutions *Appl. Phys. Lett.* **79** 4503–5
[11] Stalder K R, McMillen D F and Woloszko J 2005 Electrosurgical plasmas *J. Phys. D: Appl. Phys.* **38** 1728–38
[12] Dunaevsky A *et al* 1999 Electron ion emission from the plasma formed on the surface of ferroelectrics. II. Studies of electron diode operation with a ferroelectric plasma cathode *J. Appl. Phys.* **85** 8474–84
[13] Dunaevsky A *et al* 1999 Electron ion emission from the plasma formed on the surface of ferroelectrics. I. Studies of plasma parameters without applying an extracting voltage *J. Appl. Phys.* **85** 8464–73
[14] Hibino M, Itoh H and Kinosita K 1993 Time courses of cell electroporation as revealed by submicrosecond imaging of transmembrane potential *Biophys. J.* **64** 1789–800
[15] International Electrotechnical Commission 2000 *IEC 60601-2-2 EN 60601-2-2. Medical Electrical Equipment - Part 2-2: Particular Requirements for the Safety of High Frequency Surgical Equipment*
[16] Neumann J and Brinkmann R 2005 Boiling nucleation on melanosomes and microbeads transiently heated by nanosecond and microsecond laser pulses *J. Biomed. Opt.* **10** 024001
[17] Joshi R P and Schoenbach K H 2000 Electroporation dymanics in biological cells subjected to ultrafast electrical pulses: a numerical study *Phys. Rev.* E **62** 1025–33
[18] Malmivuo J and Plonsey R 1995 *Strength-Duration Relation, in Bioelectromagnetism. Principles and Applications of Bioelectric and Biomagnetic Fields* (New York: Oxford University Press) pp 62–5
[19] Sivukhin D V 1977 Electricity *General Course of Physics* vol 3 (Moscow: Nauka) pp 97–9